Electronic Supplemental Information

"Double exchange in a mixed-valent octanuclear iron cluster, $[Fe_8(\mu_4\text{-}O)_4(\mu\text{-}4\text{-}Cl\text{-}pz)_{12}Cl_4]^-$."

Ekaterina M. Zueva,[a,b] Radovan Herchel,[c] Serguei A. Borshch,[d] Evgen V. Govor,[e] W. M. C. Sameera,[a] Ross McDonald,[f] John Singleton,[f] Jurek Krzystek,[g] Zdeněk Trávníček,[c] Yiannis Sanakis,[h] John E. McGrady,[a,*] and Raphael G. Raptis[e,*]

S1. High-frequency, high-field EPR spectroscopy.

The high-frequency EPR spectra of $[Bu_4N][Fe_8(\mu_4\text{-}O)_4(\mu\text{-}4\text{-}Cl\text{-}pz)_{12}Cl_4]$ at 108, 224 and 324 GHz at 10 K shown in Figure S1 feature fully isotropic resonances with g = 1.976(3), consistent with the previously reported X-band spectrum (Zueva, E. M. et al. *Inorg. Chem.* **2011**, *50*, 1021–1029). Linewidth analysis places an upper limit of 0.008 on the g-scale to the anisotropy, indicating that anisotropy is minimal despite the formal presence of a high-spin d^6-center. As a result, anisotropy is ignored in the development of spin Hamiltonians for this compound.

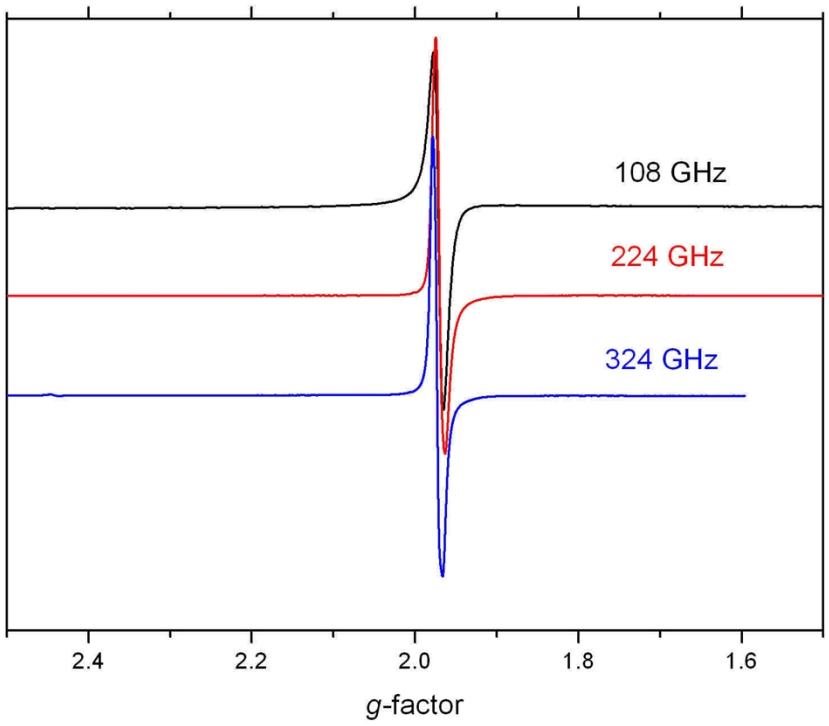

Figure S1. HFEPR spectra of $[Fe_8(\mu_4\text{-}O)_4(\mu\text{-}4\text{-}Cl\text{-}pz)_{12}Cl_4]^-$ measured at 10 K, plotted as a function of the *g*-factor. The resonant field at 108 GHz corresponds to 3.9132 T, at 224 GHz to 8.1244 T, and at 324 GHz to 11.7342 T.

S2. Ab initio computation of the spin Hamiltonian parameters.

In order to provide an initial assessment of the extent of delocalization of the itinerant electron, we have explored the spin-density distribution in the state of maximum multiplicity, S = 39/2. The Kohn-Sham orbital for the single spin-β electron (Figure S2a) is localized primarily within the cubane core, although delocalization tails on the Fe_o sites are apparent in the contour plot. This provides an early indication that both transfer pathways, cubane-cubane (described by parameter t_1) and cubane-outer (described by parameter t_2), should be important in modelling of the magnetic data.

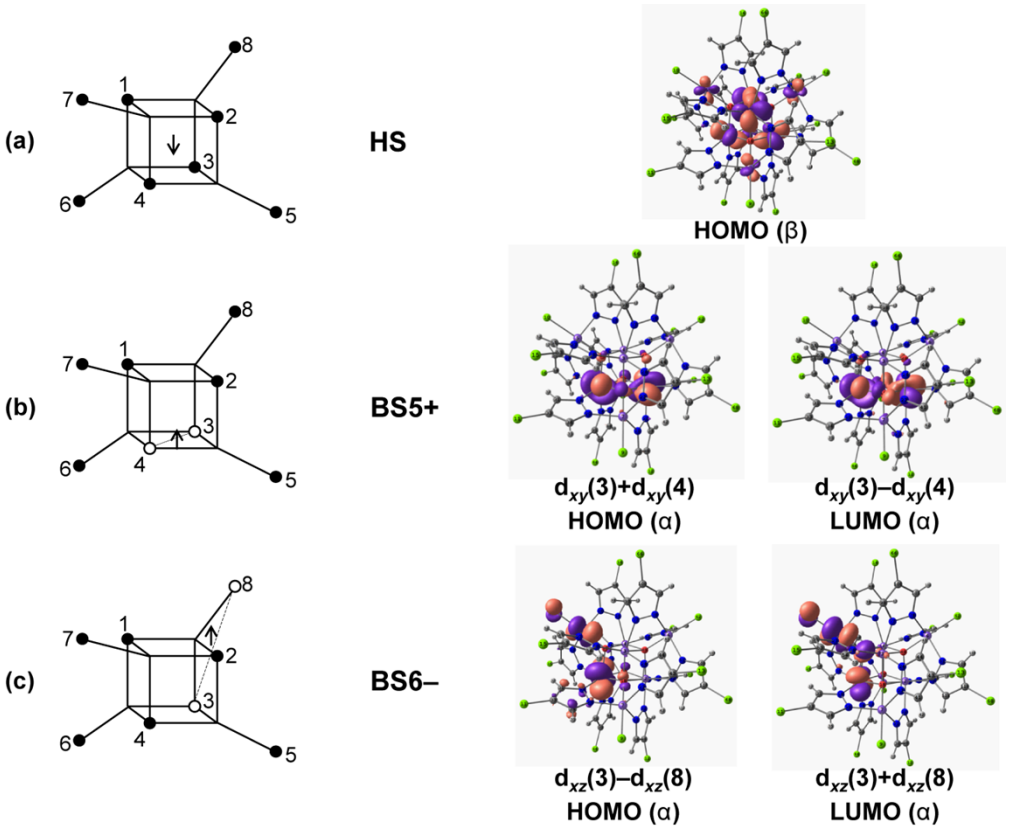

Figure S2. Kohn-Sham orbitals for the HOMO of the HS state (a) and the HOMO and LUMO of the ground BS5 (b) and BS6 (c) states ($BS5_+$ and $BS6_-$).

From the frontier orbitals of BS5 and BS6 states (Figure S2b,c) it can be seen that different orbitals on the Fe_c sites are involved in the cubane-cubane and cubane-outer transfer pathways (d_{xy} and d_{xz}, respectively). Thus, we generated two distinct versions of BS1 states and two distinct versions of BS3 states, one where the itinerant electron occupies the d_{xy}-based orbital and the other the d_{xz}-based one. The set of spin Hamiltonian parameters that arises from occupation of the d_{xy}-based orbital is presented in the paper, but the alternative *xz* parameters (J_1 = –4.0 cm^{-1}, J_2 = –12.6 cm^{-1}, J_3 = –57.0 cm^{-1}, Δ = 0.8 cm^{-1}) do not differ by more than 2.5 cm^{-1}.

The sign of Δ (> 0) is consistent with the amplitudes of the HOMO and LUMO in the ground BS6 state (Figure S2c) where the former is polarized marginally towards the Fe_c site, indicating that it is energetically more stable. Our estimate of Δ is probably a lower limit due to the use of the near *T*-symmetric X-ray geometry for the DFT computations. Larger values

of Δ result in somewhat smaller values of t_2, but the differences are not significant (for example, t_2 = 1464 cm^{-1} for Δ = 2000 cm^{-1}).

As a test of the DFT-computed spin Hamiltonian parameters we can return to the HS (S = 39/2) state, which is well described by a single Kohn-Sham determinant. For states with the maximum multiplicity, S = 39/2, the spin Hamiltonian matrix has a particularly simple structure as all diagonal and nondiagonal blocks are reduced to one element. In the case of t_1 < 0 (confirmed by our electronic structure analysis), the lowest root of this matrix is nondegenerate and can be associated with the HS (S = 39/2) state computed by DFT. The separations between the eigenvalues and the coefficients of the eigenvectors depend primarily on t_1 and t_2, but also on J_1, J_2 and Δ. For the parameter set {t_1 = –1438 cm^{-1}, t_2 = 1784 cm^{-1}, J_1 = –5.9 cm^{-1}, J_2 = –10.1 cm^{-1}, Δ = 0.7 cm^{-1}}, the excited roots are well separated and should not be populated even at room temperature, and the coefficients of the lowest eigenvector indicate that the itinerant electron is 68% localized within the cubane core, 32% within the outer sphere. This distribution is fully consistent with the amplitudes of the spin-β Kohn-Sham HOMO shown in Figure S2a.

S3. Development of spin Hamiltonians.

Clemente-Juan, J. M. *et al.* (*Inorg. Chem.* **2009**, *48*, 4557–4568) have proposed a model Hamiltonian based on a smaller hexanuclear cluster (Equations S1 and S2, Scheme S1).

$$H(6) = H_{ex} + H_{tr}$$

$$H_{ex} = -J_{1(2)} \sum_{i=1}^{3} \sum_{j>i}^{3} (\mathbf{S}_i \cdot \mathbf{S}_j) - J_{3(4)} \sum_{i=4}^{6} \sum_{j=1, j\neq i-3}^{3} (\mathbf{S}_i \cdot \mathbf{S}_j) + E_D \qquad \text{(Equation S1)}$$

$$H_{tr} = t_1 \sum_{i=1}^{3} \sum_{j=1, j\neq i}^{3} H_{tr}(i \rightarrow j) + t_2 \sum_{i=4}^{6} \sum_{j=1, j\neq i-3}^{3} H_{tr}(i \rightarrow j) \qquad \text{(Equation S2)}$$

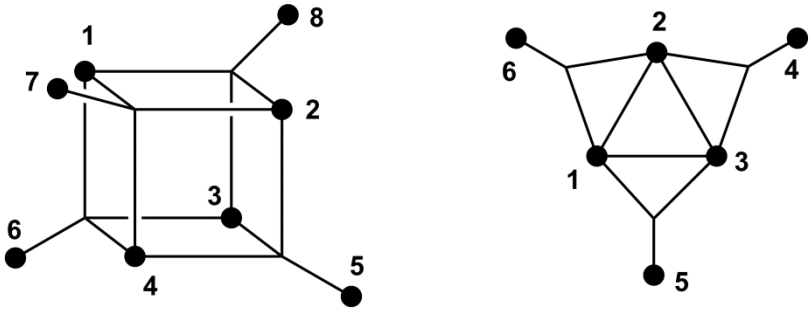

Scheme S1. Labelling schemes for the octa- and hexanuclear spin Hamiltonians used to interpret the magnetic data.

In the limiting case where $t_2 = 0$, the energy patterns have been shown ($J_1 = J_2$, $J_3 = J_4$) to be very similar in both clusters. The authors anticipated a negative value of t_1, which, in combination with the values of the isotropic exchange parameters reported for the all-ferric case in our original paper, leads to the prediction of an $S = 1/2$ ground state.

In order to assess the utility of the $H(6)$ Hamiltonian in the modelling of the experimental data, we have calculated magnetic functions, again in the limiting case where $t_2 = 0$ for both octa- (top) and hexanuclear (bottom) models (Figure S3). Specifically, we compare the experimental data ($\mu_{\text{eff}}(T)$ and $M_{\text{mol}}(B)$) against values computed using three sets of parameters (red, blue and black lines) chosen to sample reasonable deviations from the DFT-computed set. In all cases, g is set equal to 2.0 (the value of 1.976 obtained from the EPR experiment produces essentially identical curves for the magnetic functions). The results confirm that the two models generate functions with very similar features: the ground state has $S = 1/2$ in both cases and the low-energy region of the eigenvalue spectrum is very similar. Interestingly, neither $\mu_{\text{eff}}(T)$ nor $M_{\text{mol}}(B)$ are sensitive to t_1. In the plots of $M_{\text{mol}}(B)$, the three lines are indistinguishable. However, the results for both models deviate significantly from the experimental data, suggesting that the cubane-outer electron transfer, t_2, plays a significant role.

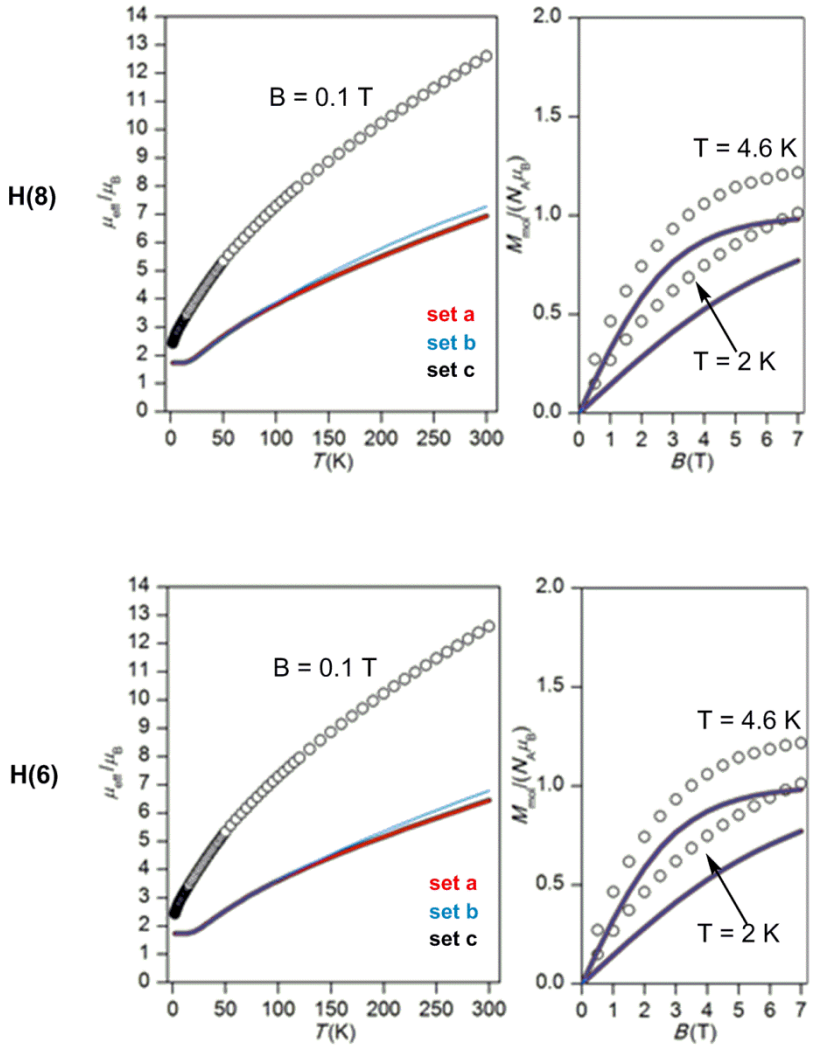

Figure S3. Plots of measured $\mu_{\text{eff}}(T)$ at B = 0.1 T and $M_{\text{mol}}(B)$ at T = 2 and 4.6 K for $[Fe_8(\mu_4\text{-}O)_4(\mu\text{-}4\text{-}Cl\text{-}pz)_{12}Cl_4]^{-}$ (open circles). The calculated lines correspond to spin Hamiltonians based on the octanuclear (top) and hexanuclear (bottom) clusters, respectively. The following parameter sets are used: (a) $J_1 = -5.9$ cm^{-1}, $J_2 = -10.1$ cm^{-1}, $J_3 = J_4 = -55.1$ cm^{-1}, $t_1 = -1438$ cm^{-1}, $t_2 = 0$; (b) $J_1 = J_2 = 0$, $J_3 = J_4 = -55.1$ cm^{-1}, $t_1 = -1438$ cm^{-1}, $t_2 = 0$; (c) $J_1 = -5.9$ cm^{-1}, $J_2 = -10.1$ cm^{-1}, $J_3 = J_4 = -55.1$ cm^{-1}, $t_1 = t_2 = 0$. In all cases, $g = 2.0$.

S4. Tests of the sensitivity of the magnetic functions to variations in isotropic exchange and asymmetry parameters.

The influence of the dominant cubane-outer exchange interactions (J_3 for Fe^{III}-Fe^{III} and J_4 for $Fe^{II/III}$-$Fe^{III/II}$) on $\mu_{eff}(T)$ is explored in Figure S4 where J_1, J_2, t_1 and t_2 are fixed at their DFT-computed values and J_3 (= J_4) varied systematically between 0 and –70 cm^{-1} (*cf.* the DFT-computed value for J_3 of –55.1 cm^{-1}). Increasingly antiferromagnetic cubane-outer exchange (more negative $J_{3,4}$) stabilizes low-spin states, successively changing the ground-state multiplicity from S = 29/2 (for $J_3 = J_4 = 0$) to S = 1/2 (for $J_3 = J_4 < –45$ cm^{-1}). The best agreement with the experimental $\mu_{eff}(T)$ curve is found in the region –70 $cm^{-1} < J_3 = J_4 < –45$ cm^{-1}, consistent with our computed value of –55.1 cm^{-1}.

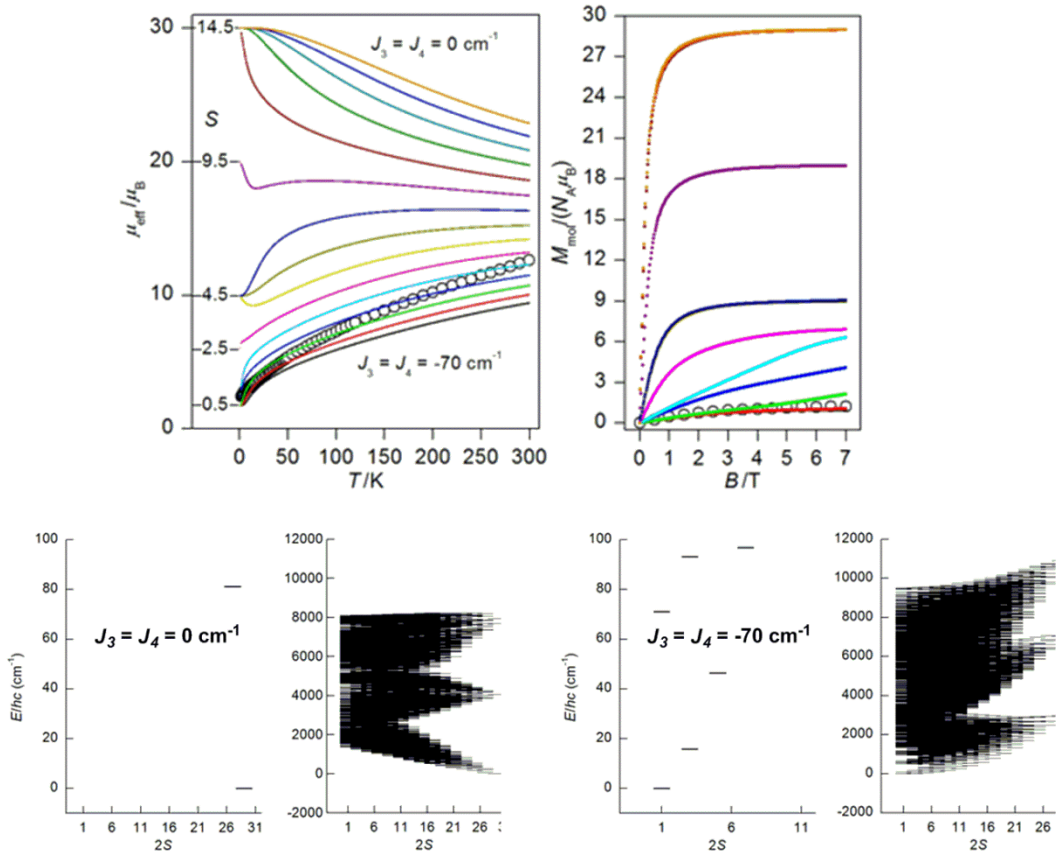

Figure S4. Plots of $\mu_{eff}(T)$ at B = 0.1 T and $M_{mol}(B)$ at T = 2 K for the hexanuclear cluster: J_1 = –5.9 cm^{-1}, J_2 = –10.1 cm^{-1}, t_1 = –1438 cm^{-1}, t_2 = 1784 cm^{-1} (all fixed), $J_3 = J_4$ varies from 0 to –70 cm^{-1} in steps of 5 cm^{-1}, g = 2.0, Δ is set to zero.

Equally, the intrinsic site asymmetry stabilizes low-spin states and reduces the influence of the cubane-outer double exchange (Figure S5). Note, however, that the effect is not pronounced. The use of a smaller value of t_2 = 1464 cm^{-1}, obtained from the BS6-matrix for Δ = 2000 cm^{-1} (see S2), results in a further decrease in μ_{eff}.

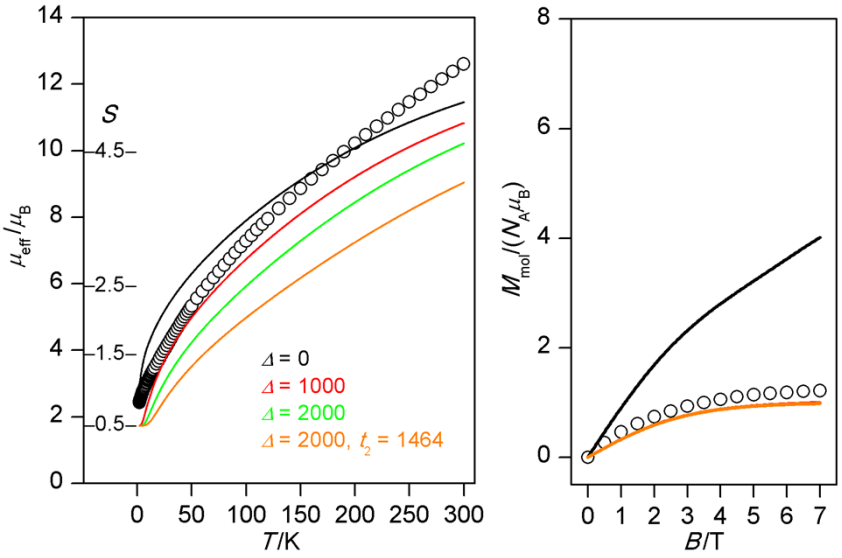

Figure S5. Plots of $\mu_{eff}(T)$ at B = 0.1 T and $M_{mol}(B)$ at T = 2 K for the hexanuclear cluster: J_1 = –5.9 cm^{-1}, J_2 = –10.1 cm^{-1}, $J_3 = J_4$ = –55.1 cm^{-1}, t_1 = –1438 cm^{-1}, t_2 = 1784 cm^{-1} (all fixed), Δ varies from 0 to 2000 cm^{-1} in steps of 1000 cm^{-1} (orange line corresponds to J_1 = –5.9 cm^{-1}, J_2 = –10.1 cm^{-1}, $J_3 = J_4$ = –55.1 cm^{-1}, t_1 = –1438 cm^{-1}, t_2 = 1464 cm^{-1}, Δ = 2000 cm^{-1}), g = 2.0.

The sensitivity of $M_{mol}(B)$ to variations in $J_{3,4}$ and Δ is explored in Figures S6 and S7. One can see that B_c is largely invariant to significant deviations of either the isotropic exchange or asymmetry parameters from their DFT-computed values.

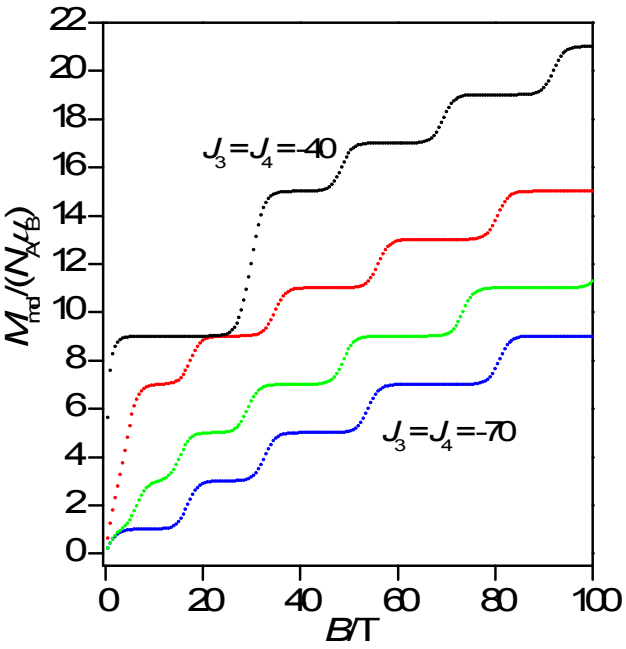

Figure S6. Simulated field dependence of the molar magnetization for the hexanuclear cluster: $J_1 = -5.9$ cm^{-1}, $J_2 = -10.1$ cm^{-1}, $t_1 = -1438$ cm^{-1}, $t_2 = 1784$ cm^{-1} (all fixed), $J_3 = J_4$ varies from –40 cm^{-1} to –70 cm^{-1} in steps of 10 cm^{-1}, $g = 2.0$, Δ is set to zero.

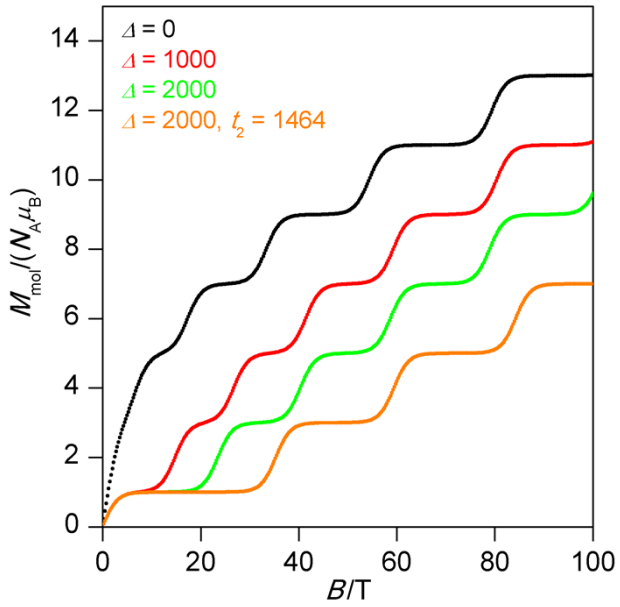

Figure S7. Simulated field dependence of the molar magnetization for the hexanuclear cluster: $J_1 = -5.9$ cm^{-1}, $J_2 = -10.1$ cm^{-1}, $J_3 = J_4 = -55.1$ cm^{-1}, $t_1 = -1438$ cm^{-1}, $t_2 = 1784$ cm^{-1} (all fixed), Δ varies from 0 to 2000 cm^{-1} in steps of 1000 cm^{-1} (orange line corresponds to $J_1 = -5.9$ cm^{-1}, $J_2 = -10.1$ cm^{-1}, $J_3 = J_4 = -55.1$ cm^{-1}, $t_1 = -1438$ cm^{-1}, $t_2 = 1464$ cm^{-1}, $\Delta = 2000$ cm^{-1}), $g = 2.0$.

S5. Sample magnetic moment versus pulsed magnetic field plots for two $[Fe_8]^0$ compounds.

For calibration purposes, we have applied the same methodology (as applied to the $[Fe_8]^-$ compound, Figure 2b) to all-ferric analogues, $[Fe_8]^0$. In this case, we observe a saturation step at 36.5 T corresponding to a ground-state crossing from $S = 0$ to $S = 1$ (Figure S8). This crossover field, B_c, corresponds to a zero-field separation $\Delta E(0–1) = g \cdot \mu_B \cdot B_c = 49.0$ K (34.1 cm^{-1}), assuming $g = 2.0$. For comparison, the eigenvalue spectrum reconstructed using our previously reported best-fit parameters for the all-ferric case indicates a singlet-triplet separation of 55.5 K (38.6 cm^{-1}).

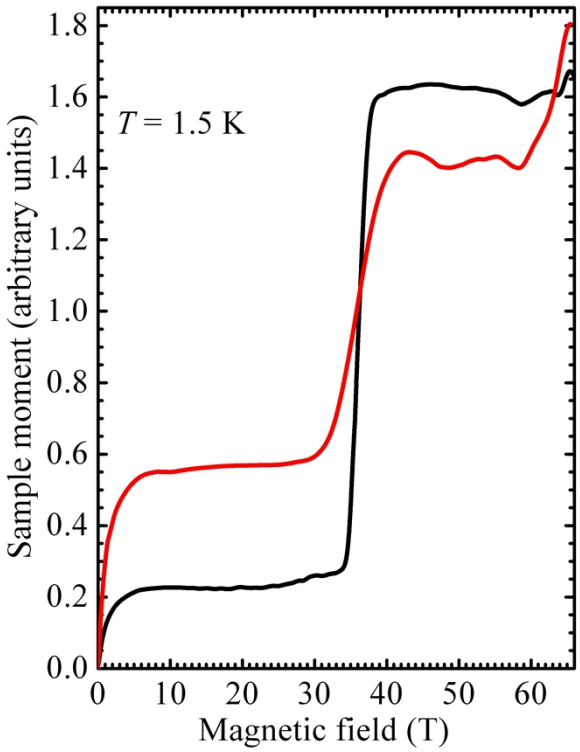

Figure S8. Sample magnetic moment vs. pulsed magnetic field plots for $[Fe_8(\mu_4\text{-}O)_4(\mu\text{-}4\text{-}Cl\text{-}pz)_{12}(NCS)_4]$ (black) and $[Fe_8(\mu_4\text{-}O)_4(\mu\text{-}4\text{-}Cl\text{-}pz)_{12}Br_4]$ (red).